ARTICLE NO. 79-0041R

Erosion Behavior in a Simulated Jet Engine Environment

T. Wakeman* and W. Tabakoff†
University of Cincinnati, Cincinnati, Ohio

This paper presents erosion data relevant to gas turbine engines. Data were obtained in a material erosion facility for Ti 6-4 and INCO 718 alloys, for temperatures between ambient and 1300°F, particle velocities between 200 and 900 ft/s, and particle impingement angles between 20 and 90 deg. These data indicate that the erosion rate as a function of temperature is relatively constant for each material up to a temperature which is unique to the material, beyond which it increases rapidly. Further, the angle dependence of erosion rate remains relatively constant with increasing material temperature.

Introduction

In many industrial and military applications, the erosive action of high-speed particles results in serious problems. Erosion has been pointed out as a problem in such diverse areas as gas turbines, rocket nozzles, coal-fired boiler systems, etc. Recent interest into this old problem coincides with increased usage of gas turbines in dusty terrains. The cost of maintaining such engines in dusty environments is great. Air filtration has alleviated the problem somewhat, but filtration reduces both payload and engine performance. If erosion can be incorporated as an engine design parameter, perhaps an erosion-tolerant engine can be produced.

Two problems are involved in erosion prediction. First, the velocity, direction, and number of particles striking the surface must be determined. These are naturally affected by the general and local flow conditions. The second part involves the calculation of the surface material removed using the information obtained from the first part. The problem of predicting erosion in rotating machinery is particularly complicated by multiple impacts.[1]

Present State of the Art

The theoretical studies concerning erosion are predominantly empirical. They involve basic assumptions as to the process governing material removal. Finnie[2] and Smeltzer et al.[3] have conducted theoretical analyses of the erosion of ductile materials. In more recent investigations,[1,4,5] further insight into the actual mechanism of erosion has been obtained by examining the target surface at high magnification using metallographic techniques and electron microscopy. A detailed description of these test facilities at the University of Cincinnati's Propulsion Laboratory can be found in Refs. 1 and 6.

In many turbomachinery applications, erosion takes place at elevated temperatures neaer the strength limiting temperatures of the materials used. For example, even in the case of turbojet engine compressors, titanium used in the early stages and the INCO 718 used in the aft stages are operated at metal temperatures in excess of 316 and 593°C (600 and 1100°F), respectively. In both cases, these temperatures are very close to the maximum operating temperatures used for these materials. The erosion characteristics can significantly change under elevated temperatures, as evidenced in the data presented by Tabakoff and Hamed.[6] These data were obtained with the sample heated to temperatures up to 204°C (400°F). Although this temperature falls far short of those experienced in turbine engines, it still indicates the significant effect of temperature on erosion and probably on the rebound characteristics.

Received Dec. 4, 1978; presented as Paper 79-0041 at the AIAA 17th Aerospace Sciences Meeting, New Orleans, La., Jan. 15-17, 1979; revision received May 21, 1979.

Index categories: Structural Stability; Thermal Stresses.

*Graduate Research Assistant, Dept. of Aerospace Engineering and Applied Mechanics.

†Professor, Dept. of Aerospace Engineering and Applied Mechanics. Associate Fellow AIAA.

High-Temperature Erosion Rig

An erosion test facility was designed to provide erosion and rebound data in the range of operating temperatures experienced in compressors and turbines. For that purpose, this facility has been designated to operate at a test section temperature in the range of ambient to 1093°C (2000°F). In addition to high temperatures, the facility properly simulates all erosion parameters which were found to be important from previous testing at ambient temperatures. These parameters include particle velocity, angle of impact, particle size, particle concentration, and sample size. Close attention was given to aerodynamic effects to insure that important parameters, such as angle of attack, are not masked or altered.

General Description of the Erosion Rig

The schematic of the test apparatus, is shown in Fig. 1, consists of the following components: particle feeder (A), main air supply pipe (B), combustor (C), particle preheater (D), particle injector (E), acceleration tunnel (F), test section (G), and exhaust tank (H).

The equipment functions as follows: A measured amount of abrasive grit of a given constituency is placed into the particle feeder (A). The particles are fed into a secondary air source and blown up to the particle preheater (D), and then to the injector (E) where it mixes with the main air supply (B), which is heated by the combustor (C). The particles are accelerated by the high-velocity air in a constant area duct (F), which is steam cooled before impacting the specimen in the test section (G). Past the test section, the particulate flow is mixed with the coolant and dumped in the exhaust tank.

The important individual components of the high-temperature erosion facility will be described. Each component was designed with cost, maintainability, availability, and functionality as prime considerations.

Particle Feeder Assembly (A)

The particles from the feeder are blown up to the particle injector area. The feeder is designed as a pressure vessel to operate at high air pressures. However, this pressure is equalized above and below the plunger by a bypass line. This

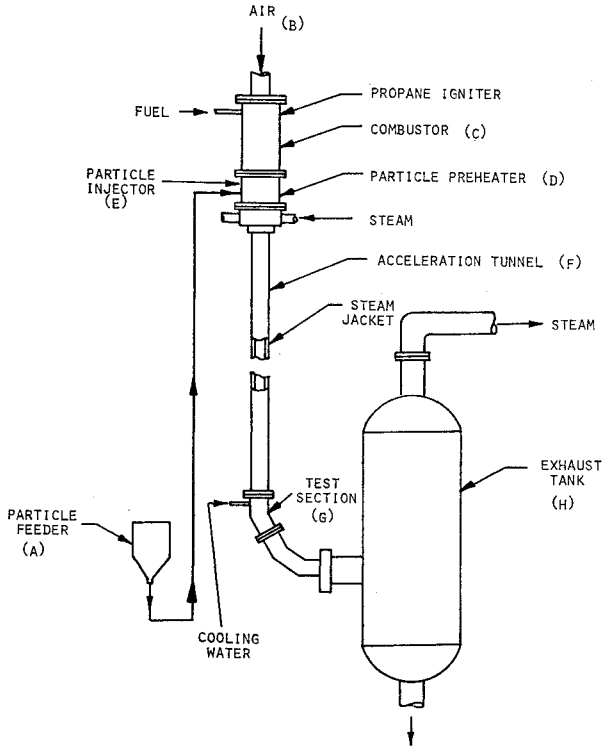

Fig. 1 Schematic of erosion test facility.

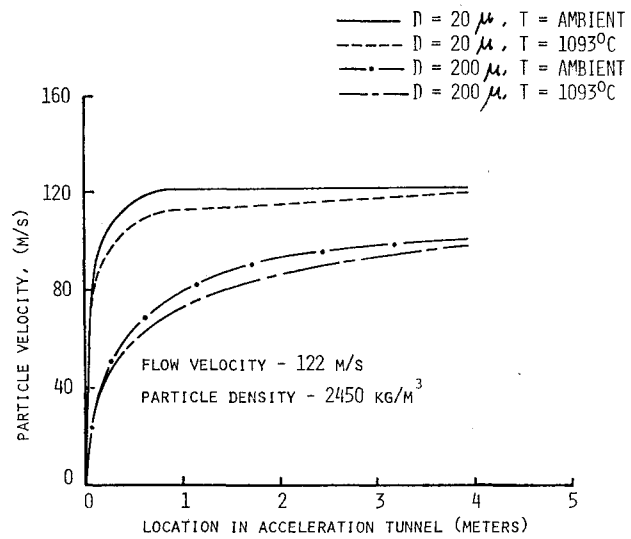

Fig. 2 Particle dynamics in a constant area acceleration tube.

allows the system to be calibrated under gravity feed conditions.

Combustor (C)

High-temperature combustion products are supplied by a modified General Electric J93 can combustor.

Particle Preheater (D) and Injector (E)

The preheater consists of a coil contained in a 203.2 mm (8 in.) i.d. pipe section with a distributor/injector to provide a well-distributed preheated particle supply. The particles are blown up to the accelerating section of the tunnel by secondary air, which flows from the particle feeder and passes through the preheater coils. The particles are distributed in the main airstream through their impingements on a specially contoured ball. It was observed that the particles impinging on this ball did not fragment. The particle gas mixture is accelerating through an elliptical nozzle to the acceleration section.

Table 1 Composition of sample materials and heat treat conditions of INCO 718

	Ti 6-4[a]		INCO 718[b]
Al	6.2%	Cr	19.0%
V	3.95%	Cb + Ta	5.1%
Fe	0.12%	Mo	2.95%
O	0.11%	Ti	1.0%
N	0.025%	Al	0.5%
Others	0.40% max.	Ni	52.5%
Ti	Balance	Cu	0.5%
		Si	0.3%
		C	0.1% max.
		Fe	Balance

[a]No heat treat (as received from mill). [b]Heat treat 1700°F-1 h air cool; at 1325°F-8 h furnace cool at 100°F/h to 1150°F-8 h air cool.

Acceleration Section (F)

The acceleration tunnel has a rectangular cross section of 89 × 25.4 mm (3½ × 1 in.) which is 3.66 m (12 ft) long. This section is steam cooled to minimize the heat losses. With this type of cooling, the 316 stainless-steel liner operates at a maximum of 760°C (1400°F). This results in a drop in the gas stream temperature of about 93°C (200°F). The use of water as a coolant would have resulted in at least three time the heat loss and an unacceptable gas stream temperature drop in this section.

The particle velocities attained in this acceleration section were predicted analytically and verified by experimental methods. Pressure measurements at the inlet, midsection, and exhaust were used to account for the tunnel friction when calculating the fluid velocity variation in this section. These velocities were used in calculating the particle velocities due to their acceleration by the gas stream. The calculated particle velocities are shown in Fig. 2 in the case of low fluid velocity of 122 m/s (400 ft/s) at 1093°C (2000°F) and at ambient temperature. From this figure it can be seen that the particle velocity is an exponential function of tunnel length. The law of diminishing returns would dictate that a tunnel length of 0.6–0.92 m (2-3 ft) would be sufficient for both relatively large and small particles (200 and 20 μ). A tunnel length of 3.66 m (12 ft) was chosen, however, for several theoretical and practical reasons.

Test Section (G)

The test section is designed such that the particle-laden air is channeled over the specimen and the aerodynamics of the fluid surrounding the test sample are preserved. The test specimen can be oriented at different angles to the gas stream by rotating the specimen holder. The test section is water cooled. The coolant water is discharged into the particulate gas stream at the downstream end of the test section.

Test Model

The previously described erosion test facility was used to obtain basic erosion data for two sample materials—Ti 6-4 and INCO 718. Detailed analysis of these two materials, as well as the heat treat conditions, are given in Table 1.

The material erosion was determined from the weight of the 19.0 × 25.4 mm specimen and after testing. The abrasive particles used consisted of quartz sand (SiO_2) obtained from commercial suppliers. The sand was sifted to obtain a particle size range of 150-180 μ. The experimental measurements were obtained for sand-particle velocities varying from 200 to 900 ft/s and target temperature varying from ambient to 1300°F, approximately 10% of the test points were repeated and the test facility was calibrated at approximately 100 test-point

intervals to assure uniformity of data. Several test points were accumulated with no particle injection resulting in no significant change in sample weight. Significant oxidation and corrosion of the samples were not expected, due to the short duration (5 min at test temperature).

It is well known from previous testing that particle velocity, particle impingement angle, aerodynamic effects, and the material sample temperature strongly influence the erosion rate. These parameters were varied in the present test program. Parameters of second importance, such as particle size, sample size, particle concentration, and sample heat treat conditions, were held constant in this investigation.

Particle velocity was controlled by varying the tunnel airflow. The particle impingement angle was set by rotating the sample relative to the flow stream direction. Sample temperature was varied by heating the flow stream which heated the material sample to the desired temperature. Aerodynamic effects are preserved by the test section tunnel design. Flow conditions in the tunnel provide the aerodynamics around the blades sample.

Test data were accumulated by setting the particle impingement angle at 20, 25, 45 and 90 deg; the sample temperature and the particle velocity. The experimental data were then plotted primarily vs velocity with angle of attack and temperature. Cross plates were made to show the effect of the angle of attack and the material sample temperature on the erosion rate.

Experimental Results and Discussion

Effect of Particle Velocity

Particle velocity was found to have a powerful effect on erosion rates. In all cases investigated, the erosion rate was shown to be proportional to the particle velocity taken to a constant power. This is similar to the results found by earlier investigators. Erosion rate vs particle velocity data for Ti 6-4 is displayed in Figs. 3-6. On each figure, the volumetric erosion rate is plotted vs particle density for different sample temperatures. Each figure represents a different particle impingement angle. For Ti 6-4, the erosion rate is shown to be proportional to the particle velocity to the n power, when n represents the slope of the straight lines on these figures. The range of n is dependent on the angle of attack and the sample temperature.

Erosion rate data for INCO 718 are similarly plotted on Figs. 7-10. Similar to Ti 6-4, the erosion rate was found to be proportional to particle velocity, taken to a power with the exponent a function of both sample temperature and impingement angle.

Both materials tested exhibited similar characteristics with the velocity exponent tending to increase with increasing impingement angle and decrease with increasing sample temperatrure. It is interesting to note the wide range of the exponent values for any one material. This variation has been shown to be related to the particle velocity restitution ratio in Ref. 1. Apparently, both increases in impingement angle and sample temperature affects the erosion rate.

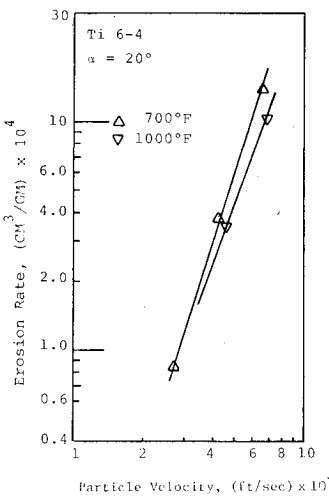

Fig. 3 Ti 6-4 erosion rate vs particle velocity for different sample temperatures, $\alpha = 20$ deg.

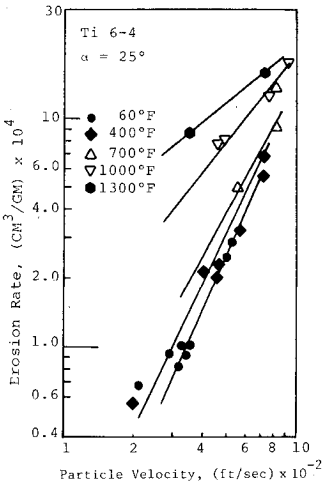

Fig. 4 Ti 6-4 erosion rate vs particle velocity for different sample temperatures, $\alpha = 25$ deg.

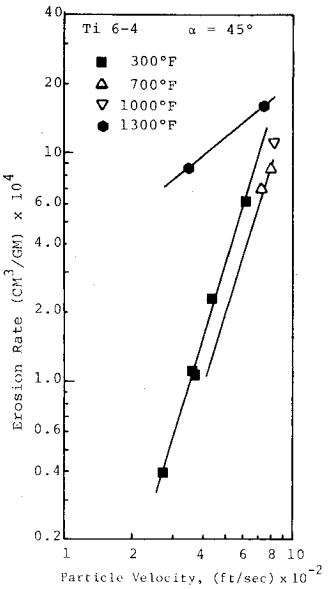

Fig. 5 Ti 6-4 erosion rate vs particle velocity for different sample temperatures, $\alpha = 45$ deg.

Effect of Sample Temperature

The erosion rate vs the sample temperature is presented in Figs. 11 and 12 for the two other materials being considered. The results in these figures are for a particle velocity of 500 ft/s, and are cross plotted from the erosion rate vs particle velocity curves presented earlier. Erosion rate vs sample temperature showns a slightly different trend for Ti 6-4, as shown in Fig. 11. The erosion rate increases slowly as the sample temperature is increased from room temperature to 800°F for 25 and 45 deg particle impingement angles. As the sample temperature is increased above 800°F, the erosion rate increases rapidly. The erosion rate shows a much slower rate of increase for Ti 6-4 at an impingement angle of 90 deg as sample temperature is increased. Inspection of Fig. 12 shows that the erosion rate for INCO 718 increases slowly or stays constant up to a sample temperature around 900°F, then increases abruptly as the sample temperature increases. This trend is independent of the impingement angle for INCO 718.

Effect of Particle Impingement Angle

It is well known that erosion rate is a function of particle impingement angle. For ductile materials, erosion rate in-

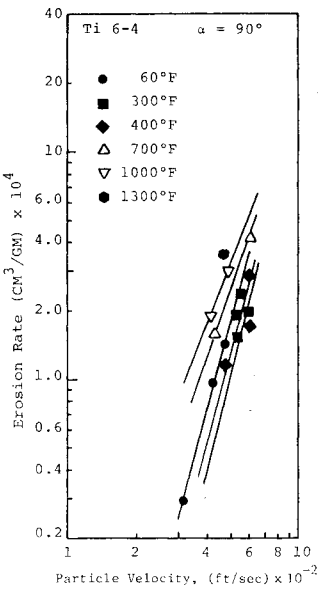

Fig. 6 Ti 6-4 erosion rate vs particle velocity for different sample temperatures, $\alpha = 90$ deg.

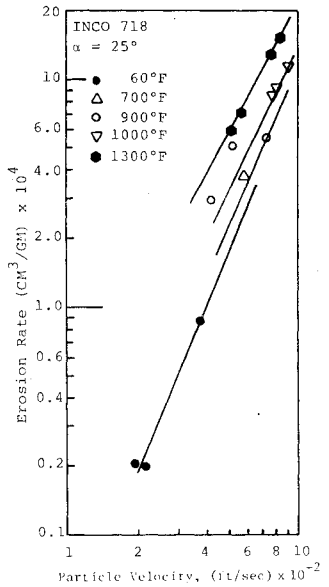

Fig. 7 INCO 718 erosion rate vs particle velocity for different sample temperatures, $\alpha = 25$ deg.

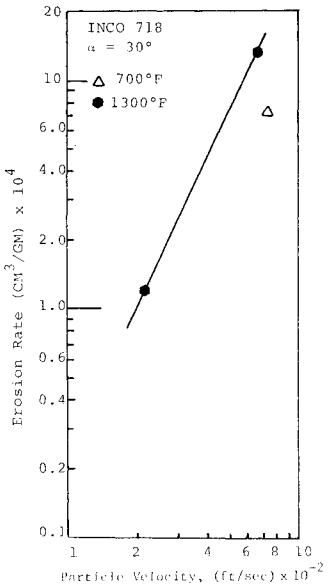

Fig. 8 INCO 718 erosion rate vs particle velocity for different sample temperatures, $\alpha = 30$ deg.

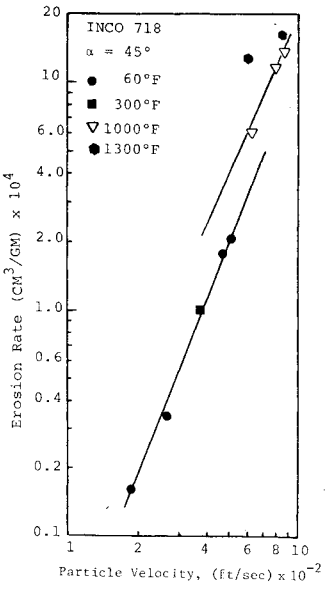

Fig. 9 INCO 718 erosion rate vs particle velocity for different sample temperatures, $\alpha = 45$ deg.

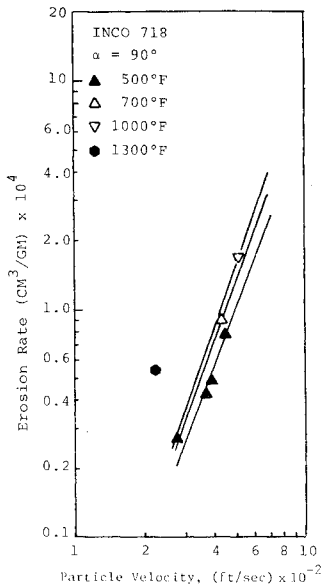

Fig. 10 INCO 718 erosion rate vs particle velocity for different sample temperatures, $\alpha = 90$ deg.

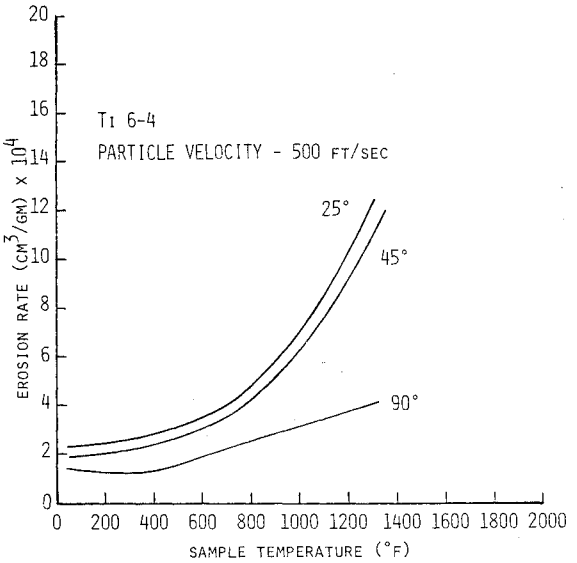

Fig. 11 Erosion rate vs sample temperature, for Ti 6-4, $\alpha = 25$, 45, and 90 deg.

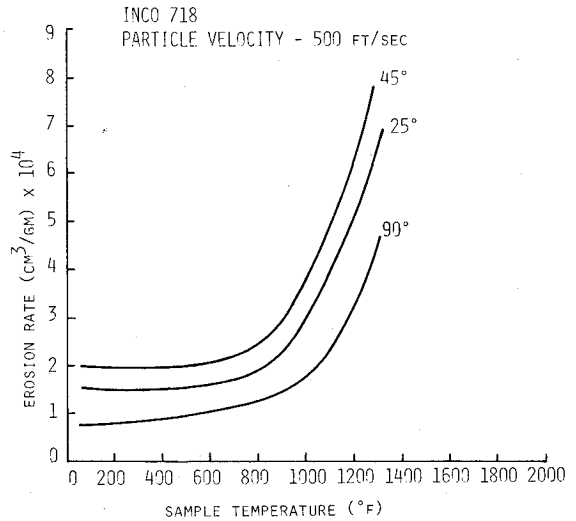

Fig. 12 Erosion rate vs sample temperature, for INCO 718, $\alpha = 25$, 45, and 90 deg.

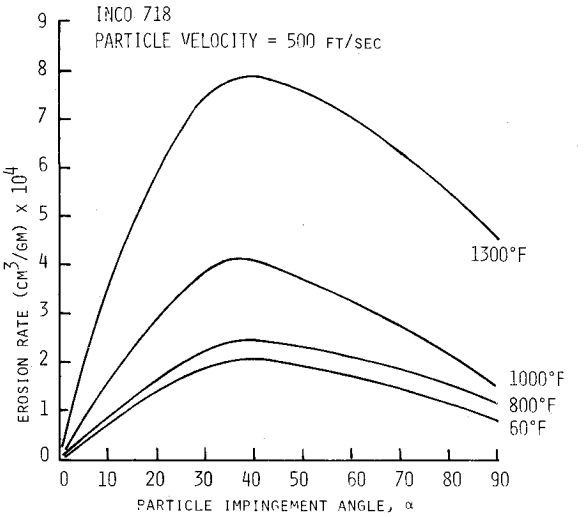

Fig. 14 INCO 718 erosion rate vs particle impingement angle for different temperatures.

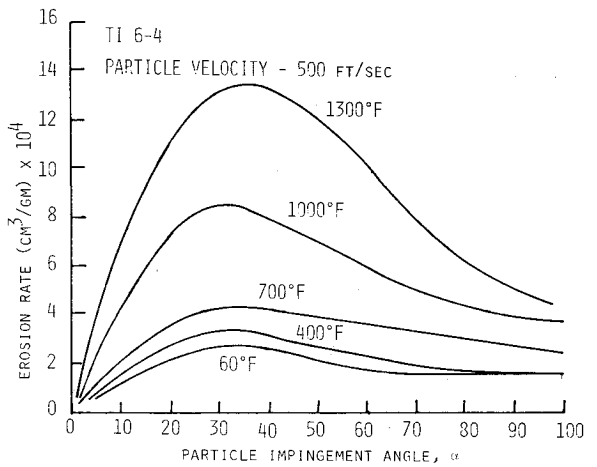

Fig. 13 Ti 6-4 erosion rate vs particle impingement angle for different temperatures.

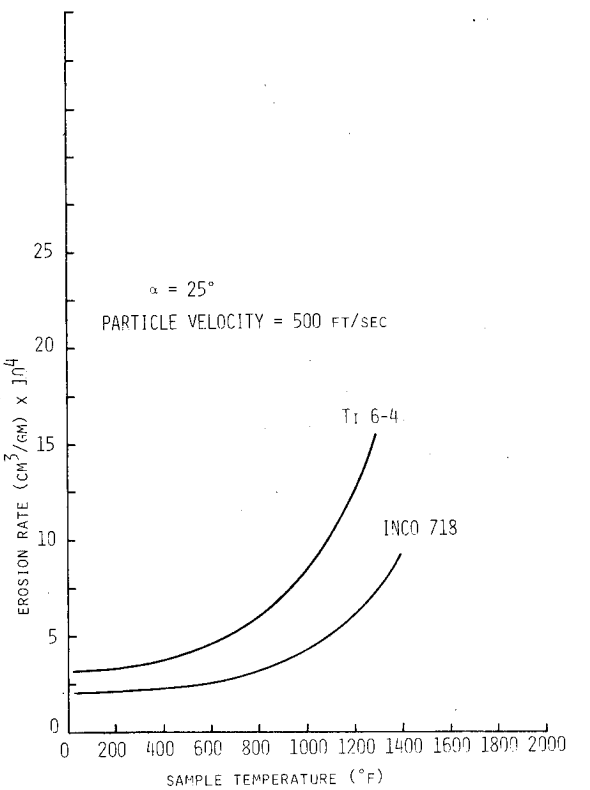

Fig. 15 Ti 6-4 and INCO 718 erosion rate vs sample temperature, $\alpha = 25$ deg.

creases from zero at a zero degree impingement angle to a maximum. After reaching a maximum, the erosion rate decreases with increasing impingement angle to a minimum value at 90 deg impingement angle.

The plots of erosion rate vs particle impingement angle presented in this paper are cross plotted from the erosion rate vs material sample temperature presented earlier. These impingement angle curves are for a particle velocity of 500 ft/s in all cases. Also, each plot of erosion rate vs impingement angle is for a constant sample temperature. The erosion rates vs the particle impingement angles for different sample temperatures are presented in Figs. 13 and 14 for Ti 6-4 and INCO 718, correspondingly. The erosion rate is a maximum for Ti 6-4 at an impingement angle of 30 deg and for the INCO 718 at 35 deg.

Effect of Sample Material

The erosion rate results presented previously show significantly different levels for the two different materials considered. An attempt was made to determine a parameter that would account for the different material properties. The erosion rate vs the sample temperature for a particle velocity of 500 ft/s and impingement angle of 25 deg is presented for the two materials in Fig. 15. From this figure, it becomes apparent that the erosion rate behaves in a similar fashion for each material. The level of erosion and the temperature where the erosion rate increases rapidly is different for each material.

In order to improve the correlation of erosion rate with the sample temperature and remove the material effect, the erosion rate was plotted vs the normalized sample temperature. In Fig. 16, the sample temperature is normalized using sample melting temperature (2920°F for Ti 6-4 and 2300°F for INCO 718). This plot does not seem a significant improvement compared with sample temperature (Fig. 15). In addition, the sample material annealed temperature (650°F for Ti 6-4 and 1750°F for INCO 718) was used as the normalizing temperature and is shown in Fig. 17. This normalization of the data gives the best correlation of the data for both materials.

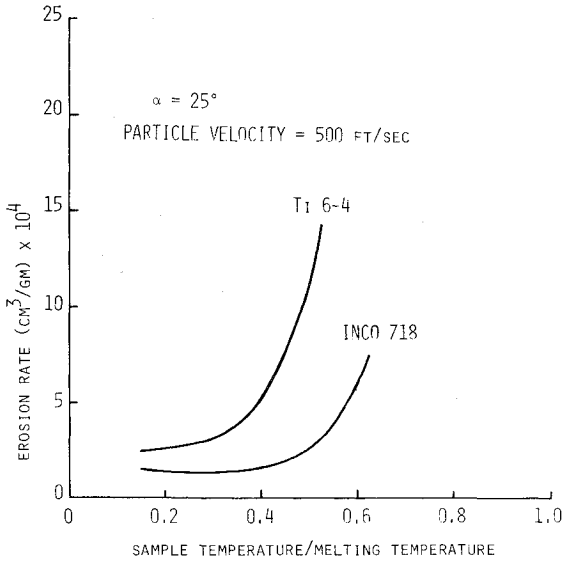

Fig. 16 Ti 6-4 and INCO 718 erosion rate vs sample temperature/melting temperature, $\alpha = 25$ deg.

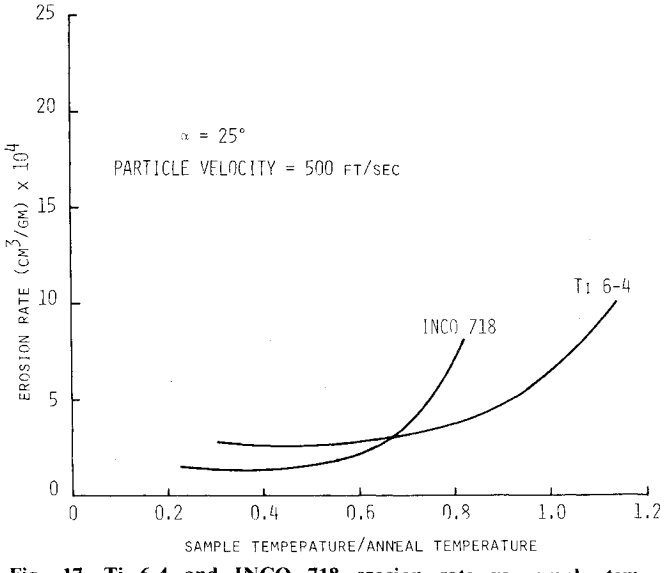

Fig. 17 Ti 6-4 and INCO 718 erosion rate vs sample temperature/anneal temperature, $\alpha = 25$ deg.

The material erosion rate has been related to material yield strength, as in Ref. 8. The annealed temperature indicates a reduction in yield strength to a low level. Figure 17 shows that the material erosion rate may be related to the annealed temperature, and that the erosion rate increases abruptly as the material sample temperature approaches the annealed temperature. This could indicate that the material erosion rate increases rapidly as the yield strength decreases rapidly near the annealed temperature. This would support the contention that material erosion rate is related to material yield strength.

Presently, we are investigating other alloys which will be used in future gas turbines. After the experimental work is completed, the data obtained will be used in developing empirical equations for predicting the erosion rates of ductile alloys at different temperatures. The empirical equations, which were developed by Grant and Tabakoff,[1] are applicable only at ambient temperatures. These relations will be used as a base for modifications to include the measured effects of higher temperatures on erosion. These modifications will incorporate the dependency of the erosion rate on the target temperature, as well as the thermal properties of the target material itself.

Conclusion

Two significant conclusions can be drawn from the data presented. Erosion rate remains relatively constant for INCO 718 and Ti 6-4 from room temperature up to a temperature unique for each material, then increases rapidly with material temperature. Also, the impingement angle at which maximum erosion occurs for each material is independent of the material sample temperature. Additionally, the velocity exponent varies considerably with changes in both the impingement angle and the material sample temperature. Ultimately, the data presented herein will be used to predict the erosion in jet engine compressors. Use of only room temperature data could yield erroneous results due to the changes in the material erosion rate with increasing material temperature.

Acknowledgment

This work was sponsored by the U.S. Army Research Office—Durham, under Contract No. DAAG-29-76-G-0229.

References

[1] Grant, G. and Tabakoff, W., "Erosion Prediction in Turbomachinery Resulting from Environmental Solid Particles," *Journal of Aircraft*, Vol. 12, May 1975, pp. 471-478.

[2] Finnie, I., Wolak, J., and Kabil, Y., "Erosion of Metals by Solid Particles," *Journal of Materials*, Vol. 2, Sept. 1967, pp. 682-700.

[3] Smeltzer, C.E., Gulden, M.E., McElmury, S.S., and Compton, W.A., "Mechanisms of Sand Dust Erosion in Gas Turbine Engines," USAAVLABS Tech. Rept., Aug. 1970.

[4] Frass, A.P., "Survey of Turbine Bucket Erosion Deposits, and Corrosion," ASME Paper 75-GT-125, presented at the Gas Turbine Conference, Houston, Texas, March 2-6, 1975.

[5] Finnie, I., "An Experimental Study on Erosion," *Proceedings of the Society for Experimental Stress Analysis,* Vol. 17, No. 2, pp. 65-70.

[6] Tabakoff, W. and Hamed, A., "Aerodynamic Effects on Erosion in Turbomachinery," JSME and ASME Paper 70, 1977 Joint Gas Turbine Congress, Tokyo, Japan, May 22-27, 1977.

[7] Tabakoff, W. and Wakeman, T., "Test Facility for Material Erosion at High Temperatures," ASTM Publication, "Erosion: Prevention and Useful Applications," STP 664, 1978.

[8] Bitter, J.G.A., "A Study of Erosion Phenomena," *Journal of Wear,* Vol. 6, 1963, Pt. I, pp. 5-21, and Pt. II, pp. 169-190.